https://doi.org/10.5194/egusphere-2025-4841
Preprint. Discussion started: 17 October 2025

The impact of CO on secondary organic aerosols formed from the mixture of α-pinene and n-dodecane

Guangzhao Xie[1], Aristeidis Voliotis[1,2], Thomas J. Bannan[1], Yunqi Shao[1], Huihui Wu[1*], Dawei Hu[1,2], and Gordon McFiggans[1]

[1]Centre for Atmospheric Science, Department of Earth and Environmental Sciences, School of Natural Sciences, University of Manchester, Manchester, M13 9PL, UK
[2]National Centre for Atmospheric Science (NCAS), University of Manchester, Manchester, M13 9PL, UK
*Now at: Univ Paris Est Créteil and Université Paris Cité, CNRS, LISA, 94010 Créteil, France

Correspondence to: Gordon McFiggans (g.mcfiggans@manchester.ac.uk) and Aristeidis Voliotis (aristeidis.voliotis@manchester.ac.uk)

https://doi.org/10.5194/egusphere-2025-4841
Preprint. Discussion started: 17 October 2025

Abstract. Atmospheric simulation chambers are powerful tools for investigating atmospheric processes and form the basis for model parameterisations. Ensuring the atmospheric relevance of experimental conditions is crucial for understanding and predicting the impacts of secondary organic aerosols (SOA) on air quality and climate. However, chamber studies are often conducted under simplified conditions, which may limit their applicability to real-world scenarios. Here, we investigated the impact of CO on the mass yields and chemical composition of SOA particles formed from a biogenic volatile organic compound (VOC, α-pinene), an anthropogenic intermediate-volatility organic compound (IVOC, n-dodecane), and their mixture in the presence of nitrogen oxides (NO_x = NO_2 + NO) in the Manchester Aerosol Chamber (MAC). This photochemical system better represents polluted atmospheric conditions. The results show that the influence of CO differed between single- and mixed-precursor systems. In the single-precursor systems, CO significantly suppressed SOA particle mass yields, whereas no such suppression was observed in the mixture. Moreover, compared with the single-precursor systems, CO exerted a diminished impact on the organic peroxy (RO_2) radical reaction pathways in the mixture, with the extent of this change differing between α-pinene and n-dodecane. These findings demonstrate that variations in reaction conditions can lead to different responses in SOA particle properties between the single- and mixed-precursor systems, highlighting the importance of conducting laboratory experiments under atmospherically relevant conditions.

https://doi.org/10.5194/egusphere-2025-4841
Preprint. Discussion started: 17 October 2025

1 Introduction

Organic aerosols (OA) account for 20 to 90% of the total atmospheric fine particulate matter mass and can significantly influence climate, air quality, and human health (Hallquist et al., 2009; Jimenez et al., 2009; Ramanathan et al., 2001). A substantial fraction of OA consists of secondary organic aerosols (SOA), which are formed through the vapour phase oxidation of gas-phase organic compounds and subsequent partitioning into the condensed phase (Atkinson and Arey, 2003; Baltensperger et al., 2005; Robinson et al., 2007). Comprehensive understanding and accurate prediction of SOA formation are critical for assessing the impacts of aerosols on global climate and regional air quality (Kenagy et al., 2024; Shrivastava et al., 2017).

Laboratory studies and atmospheric modelling are two key approaches for investigating atmospheric SOA (Burkholder et al., 2017). Model parameterisations are largely derived from laboratory studies , and the accuracy of model predictions strongly depends on the atmospheric relevance of experimental conditions (Burkholder et al., 2017; Kanakidou et al., 2005; Kenagy et al., 2024). However, many laboratory experiments are conducted under simplified rather than atmospherically relevant conditions for experimental reasons, which may introduce uncertainties in predicting SOA concentrations in atmospheric models (Kenagy et al., 2024; Shrivastava et al., 2017; Tsigaridis et al., 2014).

The ambient atmosphere comprises a complex mixture of biogenic and anthropogenic gas-phase organic compounds (Gu et al., 2021; Guenther et al., 1995). However, laboratory studies often focus on single precursors. Increasing evidence indicates that interactions among oxidation products from different sources can influence the formation of SOA. Shilling et al. (2013) observed enhanced SOA production when anthropogenic emissions from Sacramento mixed with isoprene-rich air from the foothills. McFiggans et al. (2019) demonstrated that the presence of isoprene can suppress the particle mass yield of SOA formed from α-pinene. In multi-precursor systems consisting of two monoterpenes (α-pinene and limonene), SOA formation from α-pinene was enhanced by approximately 50 %, while that from limonene was reduced by about 20 % (Takeuchi et al., 2022). More recent studies have extended to ternary mixtures comprising biogenic (α-pinene and isoprene) and anthropogenic (o-cresol) precursors (Shao et al., 2022a; Voliotis et al., 2022a). These findings suggest that simple linear combinations of SOA mass yields from individual components may lead to inaccurate estimates of total SOA formation in mixed-precursor systems.

Atmospheric trace gases such as CO and nitrogen oxides (NO_x = NO_2 + NO) can influence the oxidant levels and alter the reaction pathways of organic peroxy (RO_2) radicals, which play a central role in the formation of SOA (Atkinson, 2000; Kroll and Seinfeld, 2008; Lane et al., 2008). In laboratory studies, without adequately considering the effects of these trace gases, the fate of RO_2 radicals may differ substantially from that in the real atmosphere (Ziemann and Atkinson, 2012). The presence of CO can directly consume OH and shift the hydroperoxy (HO_2) radical/RO_2 ratio, thereby favouring the termination of RO_2 + HO_2 over RO_2 + RO_2 reactions (Lu and Khalil, 1993). McFiggans et al. (2019) showed that CO suppressed α-pinene dimer formation by a factor of two. Similarly, Baker et al. (2024) introduced CO into the α-pinene oxidation system and demonstrated that unrealistically low HO_2/RO_2 ratios can lead to significant overestimation of SOA mass yields. Under elevated HO_2/RO_2 conditions, the formation of highly oxygenated molecule (HOM) accretion products decreased by about 60 % (Baker et al., 2024). However, these studies were conducted under NO_x-free conditions. In the ambient

https://doi.org/10.5194/egusphere-2025-4841
Preprint. Discussion started: 17 October 2025

atmosphere, CO is often co-emitted with anthropogenic pollutants such as NO_x, and the termination of RO_2 radicals involves complex interactions among RO_2, NO_x, and HO_2 (Atkinson, 2000; Kroll and Seinfeld, 2008). It is therefore important to consider the effects of CO and NO_x in conjunction. NO_x governs O_3 concentrations through the photostationary state, thereby indirectly modulating OH via O_3 photolysis (Clapp and Jenkin, 2001). Under NO_x-free conditions, $RO_2 + RO_2$ and/or $RO_2 + HO_2$ reactions dominate over RO_2 + NO reactions, whereas in the presence of NO_x, RO_2 radicals can react rapidly with NO to form alkoxy (RO) radicals or organic nitrates ($RONO_2$) (Atkinson, 2003; Chen et al., 2022; Kang et al., 2025; Ziemann and Atkinson, 2012). Ng et al. (2007) observed that, in the presence of NO_x, the SOA particle mass yield of α-pinene decreased significantly from 40 % to 6.6 %. Pullinen et al. (2020) revealed that increasing NO_x concentrations led to a decrease in the fraction of α-pinene HOM-accretion products. These findings highlight the need for laboratory studies to account for the full range of atmospherically relevant conditions.

In this study, we investigated the impact of CO on the mass yields and chemical composition of SOA particles formed from a biogenic volatile organic compound (VOC, α-pinene), an anthropogenic intermediate-volatility organic compound (IVOC, n-dodecane), and their mixture, in the presence of NO_x. α-Pinene ($C_{10}H_{16}$) is the most abundant monoterpene in the troposphere and contributes significantly to the global SOA budget (Andreae and Crutzen, 1997; Lee et al., 2006). n-Dodecane ($C_{12}H_{26}$) serves as a proxy for anthropogenic IVOCs, being widely present in fuels and emitted primarily as a non-combusted hydrocarbon (Zhao et al., 2015). CO and NO_x are ubiquitous atmospheric trace gases with substantial anthropogenic sources. Experiments were conducted in the Manchester Aerosol Chamber (MAC), using a combination of online and offline instruments to characterise particle- and gas-phase compounds. This work provides new insights into SOA particle properties under polluted conditions more representative of the atmosphere.

https://doi.org/10.5194/egusphere-2025-4841
Preprint. Discussion started: 17 October 2025

100 **Table 1.** Summary of experimental conditions.

Experiment No.	Experiment Type	$[n\text{-dodecane}]_0$[a] (ppb)	$[\alpha\text{-pinene}]_0$[a] (ppb)	$[NO_x]_0$[a] (ppb)	$[precursor]_0$[a] $/[NO_x]_0$	$[CO]_0$[a] (ppb)	$[Seed]_0$[a] (μg m^{-3})	$[O_3]_{max}$ (ppb)	SOA (μg m^{-3})	SOA particle mass yields
α-Pinene experiments										
1	α-pinene	-	59.4	57	1.0	171	31.0	37.9	39.9	0.12
2	α-pinene	-	48.9	54	0.9	185	56.1	39.0	42.1	0.16
3	α-pinene + CO	-	42.7	68	0.6	8360	35.9	60.7	17.8	0.08
n-Dodecane experiments										
4	n-dodecane	160	-	281	0.6	160	37.8	103.1	177.5	N.A.[b]
5	n-dodecane	160	-	156	1.0	195	31.2	98.4	122.9	0.17
6	n-dodecane + CO	160	-	133	1.2	9261	48.2	99.1	26.3	0.05
7	n-dodecane + CO	160	-	204	0.8	9473	47.1	98.5	14.7	0.02
Mixed-precursor experiments										
8	mixture	80	24.8	160	0.9	139	34.5	85.9	71.4	N.A.[b]
9	mixture	80	27.4	121	0.6	168	36.9	76.2	63.9	0.11
10	mixture + CO	80	22.1	109	0.6	10000	45.6	93.8	67.1	0.18
11	mixture + CO	80	14.3	161	0.9	10668	37.8	109.4	50.5	0.14

[a] The subscript "0" indicates the initial concentration.

[b] N.A.: no available data.

https://doi.org/10.5194/egusphere-2025-4841
Preprint. Discussion started: 17 October 2025

2 Methodology

2.1 Experimental setup and procedure

The experiments were conducted in the 18 m^3 MAC at the University of Manchester. The chamber comprises a fluorinated ethylene propylene (FEP) Teflon bag supported by three rectangular frames. Further details of the chamber are provided in Shao et al. (2022b). Illumination was provided by a series of halogen lamps (50W/4700K MR16, Solux), two xenon arc lamps (XBO 6000W/HSLA OFR, Osram), and a UVC lamp operating at 254 nm. The liquid precursors (α-pinene, analytic standard, Sigma-Aldrich; n-dodecane, anhydrous, ≥ 99.0 %, Sigma-Aldrich) were initially injected into a heated glass bulb to facilitate vaporisation. The resulting vapours were subsequently carried into the chamber by electronic capture device-grade nitrogen (ECD N_2). NO_x was introduced from a cylinder using ECD N_2 as the carrier gas. They served as a source of OH via O_3 photolysis, thereby initiating the photochemical oxidation. The initial precursor/NO_x ratios were controlled within the range of 0.6 to1.2, while NO_2/NO ratios were maintained between 1.5 and 2.5. Seed particles with a mass concentration of 40.2 ± 8.0 μg m^{-3} were generated by nebulising aqueous ammonium sulfate solutions ($(NH_4)_2SO_4$, ACS reagent, ≥ 99.0 %, Sigma-Aldrich) using an aerosol generator. These particles provided a condensation surface for the oxidation products, thereby reducing wall losses and suppressing nucleation (Nah et al., 2017).

Each experiment typically consisted of four steps (Fig. S1):

(i) Pre-experiment: Prior to each run, a series of preparation steps were conducted, including cyclic flushing and filling with clean air at a high flow rate for approximately 1.5 h, preheating the precursor injection bulb, introducing all reactants and seed aerosols, and adjusting the chamber temperature and relative humidity to the target values (25 °C and 50 ± 5 %, respectively).

(ii) Stabilisation: The chamber was kept in the dark for 20 to 30 min with all the reactants and seed aerosols, allowing their concentrations to stabilise.

(iii) Experiment: Each photochemical experiment lasted for approximately 5 h, corresponding to four cycles of the Filter Inlet for Gases and Aerosols coupled to a Chemical Ionisation Time-of-Flight Mass Spectrometer (FIGAERO-CIMS). Each cycle spanned 1.5 h, with the first 30 min allocated to gas and particle sampling and gas-phase analysis, followed by 1 h of particle-phase analysis (described in Sect. 2.3.1). In the final cycle, the photochemical reaction was terminated after the completion of particle sampling.

(iv) Post-experiment: After the light sources were switched off, the chamber underwent cyclic flushing and filling with clean air for approximately 1 h. It was then filled with ozone at a high concentration (≥ 1 ppm) and left to soak overnight to oxidise and remove residual O_3-reacting organic species.

Table 1 summarises the key experimental conditions and results. Repeat experiments were conducted to enhance the reliability of the results and to address data gaps caused by instrument failures. Instrument availability for each experiment is listed in Table S1. Unless otherwise stated, the figures in this paper show mean values from the available repeat experiments.

2.2 Iso-reactivity conditions

OH radicals served as the primary oxidant in our experiments. To ensure comparability across systems, all experiments were initiated with iso-reactivity towards OH radicals (Voliotis et al., 2022b; Voliotis et

https://doi.org/10.5194/egusphere-2025-4841
Preprint. Discussion started: 17 October 2025

al., 2021). Specifically, the total OH reactivity was kept constant between single- and mixed-precursor systems. In the mixture, the precursor concentrations were adjusted to contribute equally to the overall OH reactivity. This approach ensured that both precursors had an equal probability of reacting with OH and producing first-generation oxidation products (Voliotis et al., 2022b; Voliotis et al., 2021). The initial reactivity was calculated using the following equation:

$$\text{Initial reactivity } (s^{-1}) = \sum C_{precursor,i} \times K_{OH,i} \quad (1)$$

where $C_{precursor,i}$ is the concentration of precursor i (molecule cm^{-3}), and $k_{OH,i}$ is the reaction rate coefficient of precursor i with OH (cm^3 $molecule^{-1}$ s^{-1}). The reaction rate coefficients for α-pinene and n-dodecane with OH are 5.33×10^{-11} and 1.32×10^{-11} cm^3 $molecule^{-1}$ s^{-1}, respectively (Atkinson, 2003; Dash et al., 2014). As α-pinene exhibits greater reactivity towards OH than n-dodecane, a higher initial concentration of n-dodecane was used to achieve iso-reactivity in the experiments. The initial CO concentration was also determined according to the principle of iso-reactivity. The reaction rate coefficient of CO with OH is 2.50×10^{-13} cm^3 $molecule^{-1}$ s^{-1} (Amedro et al., 2012).

2.3 Instrumentation

Near-real-time gas and particle composition was measured using FIGAERO-CIMS (Aerodyne Research Inc.). Precursors (α-pinene and n-dodecane) were measured in real time using a Vocus Proton-Transfer Reaction Time-of-Flight Mass Spectrometry (Vocus PTR-ToF-MS, Tofwerk). The non-refractory submicron aerosol particle composition, including aerosol sulfate, nitrate, ammonium, chloride, and organics, was measured in real time using a Compact Time-of-Flight Aerosol Mass Spectrometer (C-ToF-AMS, Aerodyne Research Inc.). NO and NO_2 were measured using a chemiluminescence NO-NO_2-NO_x analyser (Model 42i, Thermo Fisher Scientific Inc.). O_3 and CO were measured using a UV absorption O_3 analyser (Model 49C, Thermo Fisher Scientific Inc.) and a CO analyser (Model 48i, Thermo Fisher Scientific Inc.), respectively. Particle concentration was measured with a Differential Mobility Particle Sizer (DMPS) coupled to a Condensation Particle Counter (CPC, model 3775, TSI Inc.).

2.3.1 FIGAERO-CIMS

The FIGAERO system enables simultaneous characterisation of gas- and particle-phase species by sampling gases through one inlet while collecting particulate matter on a filter via a separate sampling port (Bannan et al., 2019; Lopez-Hilfiker et al., 2014). The instrument was operated in negative-ion mode using I^- as the reagent ion, generated by passing CH_3I and N_2 over a ^{210}Po radioactive source. It was run in a cyclic mode consisting of the following procedure:

(i) 30 min of gas-phase sampling and simultaneous particle collection onto a PTFE filter (2.0 µm pore size, Zefluor) both at 1 L min^{-1}. During this step, the instrument was flushed with N_2 for 0.5 min every 4.5 min to obtain the background signal.
(ii) 25 min of temperature-programmed thermal desorption of the collected particles, with the temperature ramped from ambient to 310 °C.
(iii) 15 min of isothermal soaking at 310 °C.
(iv) 20 min of cooling from 310 °C to ambient temperature.
(v) 2 min of N_2 flushing to clean the instrument.

An "instrument background" procedure was conducted weekly to correct for the particle-phase

https://doi.org/10.5194/egusphere-2025-4841
Preprint. Discussion started: 17 October 2025

background. The FIGAERO-CIMS data were analysed using the Tofware package (v4.0.0) in Igor Pro 7.0.8 (WaveMetrics©). Peak fitting was performed over the m/z range of 200 to 550 Da.

2.3.2 Vocus PTR-ToF-MS

The Vocus PTR-ToF-MS provides high-sensitivity and fast-response measurements of organic compounds without the need for pre-concentration or chromatographic separation. Compared to traditional PTR-MS, the Vocus employs a focusing ion-molecule reactor (IMR) equipped with a radio frequency (RF) quadrupole, which focuses ions along the central axis of the reactor and thereby improves ion transmission efficiency (Jensen et al., 2023; Krechmer et al., 2018; Yuan et al., 2017). An axial electric field is applied within the IMR to increase ion collision energies and suppress the clustering of ions with water molecules (Krechmer et al., 2018; Yuan et al., 2017).

In our experiments, the ion source was supplied with a 20 sccm flow of water vapor. The IMR was operated at 60 °C and 2.0 mbar, with an axial voltage of approximately 568 V and an RF amplitude of 450 V at 1.3 MHz. The reduced electric field strength (E/N) was 141 Td. Measurements were made on a 5 min cycle, consisting of a 4 min chromatography cycle and a 1 min instrumental background. Instrument calibration was conducted daily. The calibration curve for α-pinene is presented in Fig. S2. Owing to the absence of an n-dodecane gas standard, direct quantification was not feasible. Moreover, n-dodecane undergoes extensive fragmentation during ionisation, and its molecular ion signal is subjected to interference by overlapping fragments. Therefore, alternative approaches were adopted for its quantification: (i) the initial concentrations were taken as the set values (160 ppb in the single-precursor system and 80 ppb in the mixed-precursor system), and (ii) the relative consumption of n-dodecane was inferred from the signal changes of representative fragment ions. In this study, the ion $C_{10}H_{21}^+$ was selected as a marker ion of n-dodecane to track its temporal behaviour (Fig. S3). However, this ion may still be influenced by contributions from other oxidation products, which could result in an overestimation of SOA particle mass yields. Nevertheless, this uncertainty does not affect the observed effects of CO on the overall trends and relative differences in yields.

2.3.3 C-ToF-AMS

A detailed description of the C-ToF-AMS can be found in Drewnick et al. (2009). Ionization efficiency (IE) and relative ionization efficiency (RIE) calibrations were carried out using size-selected NH_4NO_3 and $(NH_4)_2SO_4$ particles. The average IE of NH_4NO_3 was determined to be 2.75×10^{-7} ions molecule^{-1}, while the RIE for NH_4^+ and SO_4^{2-} were 4.71 ± 0.24 and 1.13 ± 0.01, respectively.

In this study, the OA/sulfate correction method was applied to calibrate the SOA particle mass concentration derived from AMS measurements (Wang et al., 2018). This method assumes that the loss rate constants of OA and seed aerosols are identical, and that seed concentrations are affected solely by wall loss. The corrected particle mass concentration is given by:

$$C_{OA}(t) = \frac{C_{OA}^{SUS}(t)}{C_{seed}(t)} C_{seed}(0) \quad (2)$$

where $C_{OA}^{SUS}(t)/C_{seed}(t)$ represents the SOA-to-sulfate ratio derived from AMS measurements, and $C_{seed}(0)$ denotes the sulfate concentration at the beginning of the experiment.

https://doi.org/10.5194/egusphere-2025-4841
Preprint. Discussion started: 17 October 2025

SOA particle mass yields (Y_{SOA}) for each system were derived from SOA particle mass concentrations measure by AMS and precursor concentrations measured by PTR. It is defined as the mass of SOA particles formed per unit of precursor consumed (Gao et al., 2022):

$$Y_{SOA} = \frac{\Delta SOA}{\Delta HC} \quad (3)$$

For the single-precursor systems, ΔHC (hydrocarbon consumption) denotes the consumption of the individual precursor, whereas for the mixed-precursor system, it refers to the total consumption of all precursors.

https://doi.org/10.5194/egusphere-2025-4841
Preprint. Discussion started: 17 October 2025

3 Results

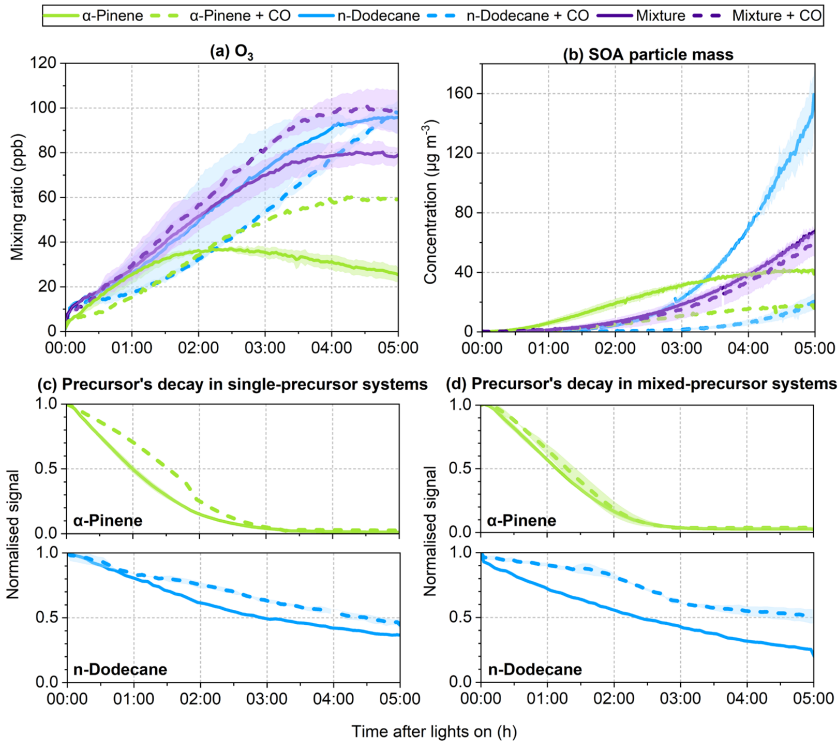

Figure 1: Time series of (a) O_3, (b) SOA particle mass concentrations, (c) and (d) normalised signal of the precursors during the photochemical reaction of α-pinene, n-dodecane and their mixture. Solid and dashed lines denote experiments conducted without and with CO, respectively. The shaded area represents the envelope of the measurements from repeat experiments.

Fig. 1 presents an overview of the temporal evolution of O_3, SOA particle mass concentrations, and precursor decay during the photochemical reactions. Solid and dashed lines represent experiments conducted in the absence and presence of CO, respectively. The corresponding time series of NO, NO_2, and CO are shown in Fig. S4. These observations form the basis for evaluating the influence of CO on SOA particle formation and mass yields across different systems. Detailed results from the α-pinene, n-dodecane, and mixed-precursor experiments are presented in the following subsections.

3.1 α-Pinene

3.1.1 SOA particle mass formation and yields

The initial O_3 concentration in the chamber was negligible. Upon illumination, O_3 gradually accumulated, peaking at 38.5 ppb approximately two hours after lights on in the absence of CO, and then declined over time. In the presence of CO, the peak O_3 concentration (60.7 ppb) was observed near the end of the experiment.

https://doi.org/10.5194/egusphere-2025-4841
Preprint. Discussion started: 17 October 2025

The initial α-pinene/NO_x ratio in the α-pinene experiments was 0.8 ± 0.2 (Table 1). In the absence of CO, NO_x concentrations declined during the first two hours of the reaction and subsequently stabilised, whereas in the presence of CO, they declined continuously throughout the experiment (Fig. S4). α-Pinene was nearly completely consumed within three hours in both experiments (Fig. 1c). Notably, its initial consumption rate was slower in the presence of CO, but increased after approximately two hours and ultimately converged with that observed in the absence of CO.

Compared to the experiment without CO, the presence of CO resulted in a slower growth rate and a substantially lower SOA particle mass concentration (Fig 1b). In both cases, the concentrations stabilised during the final hour of the reaction. By the end of the experiment, SOA particle mass concentrations reached 41.0 μg m^{-3} in the absence of CO and 17.8 μg m^{-3} in its presence. Correspondingly, the α-pinene SOA particle mass yield decreased from 0.14 to 0.08.

3.1.2 SOA particle chemical composition

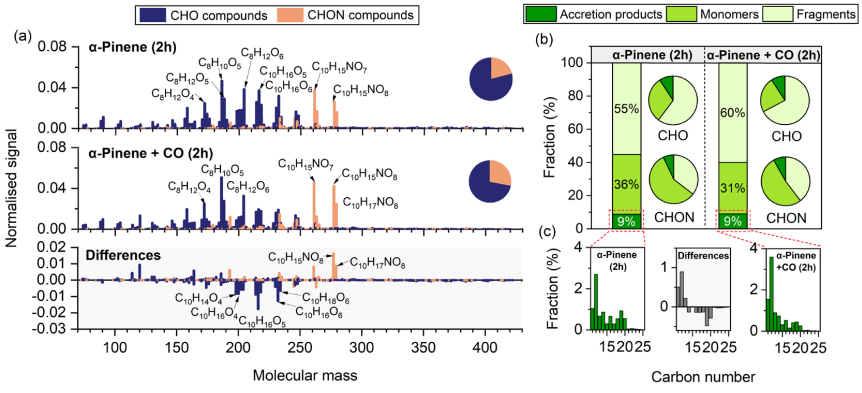

Figure 2: (a) High-resolution mass spectra of particle-phase compounds identified by FIGAERO-CIMS in α-pinene experiments conducted with and without CO, along with their differences (with CO minus without CO). All signal intensities are normalised to 1. Pie charts display the proportions of CHO and CHON compounds. (b) Fractions of α-pinene-derived fragments, monomers, and accretion products in the absence and presence of CO. Bar charts represent their contributions to the total signal, while pie charts show their relative contributions within CHO and CHON compounds. (c) Carbon number distributions of accretion products in the absence (left) and presence (right) of CO. The middle panel shows the differences between them (with CO minus without CO).

Owing to the absence of data from the final two FIGAERO cycles in the α-pinene experiment with CO, the analysis of α-pinene SOA particle composition was based on the second cycle, corresponding to two hours of reaction, by which time substantial SOA mass had already formed.

Fig. 2a presents the high-resolution mass spectra of identified SOA particles from α-pinene experiments conducted with and without CO, together with their differences. The products were mainly distributed

https://doi.org/10.5194/egusphere-2025-4841
Preprint. Discussion started: 17 October 2025

within the molecular mass range of 150 to 280 Da. According to elemental composition, the compounds were classified into CHO and CHON groups. CHON species accounted for 21 % of the total signal in the absence of CO and 28 % in its presence. In both cases, the most abundant compound was $C_8H_{10}O_5$.

The identified compounds can be categorised into three classes based on carbon number: monomers, fragments, and accretion products (Fig. 2b). Monomers derived from α-pinene consisted of C_{10} products; fragment compounds contained fewer than 10 carbon atoms, while accretion products contained more than 10. Fragment compounds were the dominant class in both the absence and presence of CO, accounting for 55 % and 60 % of the total signal, respectively. A large fraction of these fragments fell within the C_7 to C_9 range (Fig. S10). Among CHO compounds, fragments made up the largest proportion, whereas monomers dominated the CHON fraction. Notably, differences in carbon number distribution between the two systems were primarily observed in the monomer group (Fig. S10), with CO leading to a lower proportion of C_{10} CHO compounds (e.g., $C_{10}H_{16}O_{4\text{-}6}$) and higher proportion of C_{10} CHON compounds (e.g., $C_{10}H_{15}NO_{7\text{-}8}$) compared the experiment without CO (Fig. 2a). The overall contribution of accretion products remained consistent at 9 % in both systems. However, CO reduced the fraction of accretion products containing 16 to 24 carbon atoms compared to the experiment without CO (Fig. 2c).

Beyond differences in carbon number distribution, the presence of CO also altered the distribution of hydrogen atom numbers (Fig. S11). Compared with the experiment without CO, CHO compounds containing 14, 16, and 18 hydrogen atoms accounted for a lower fraction in the presence of CO. In contrast, CO led to an increase in the relative abundance of CHON compounds across full range of hydrogen atom numbers detected in this study, consistent with the observed overall increase in CHON contribution.

3.2 n-Dodecane

3.2.1 SOA particle mass formation and yields

In the n-dodecane experiments, O_3 concentrations were generally higher in the absence of CO than in its presence (Fig. 1a). The temporal evolution of O_3 differed markedly between the two systems. In the absence of CO, O_3 had nearly reached its peak by the end of the experiment, whereas in the presence of CO, O_3 levels continued to rise. Despite these differences in formation rates and peak timing, the final O_3 concentrations in both systems converged to similar levels, approaching 100 ppb.

The initial n-dodecane/NO_x ratio was 0.9 ± 0.3 (Table 1). NO_x concentrations declined steadily throughout the reaction under both conditions (Fig. S4). In the presence of CO, the consumption rate of n-dodecane was slower (Fig. 1c). By the end of the experiment, 37 % of the initial n-dodecane remained unreacted in the absence of CO, whereas 47 % remained when CO was present (Fig. 1c).

The formation rate of n-dodecane SOA particles increased throughout the experiment (Fig. 1b). In the absence of CO, 122.9 μg m^{-3} of SOA particles were produced, corresponding to a mass yield of 0.17 (exp. 5). In the presence of CO, the final SOA particle mass concentration was significantly lower, at 20.5 μg m^{-3}, with a yield of 0.04.

https://doi.org/10.5194/egusphere-2025-4841
Preprint. Discussion started: 17 October 2025

3.2.2 SOA particle chemical composition

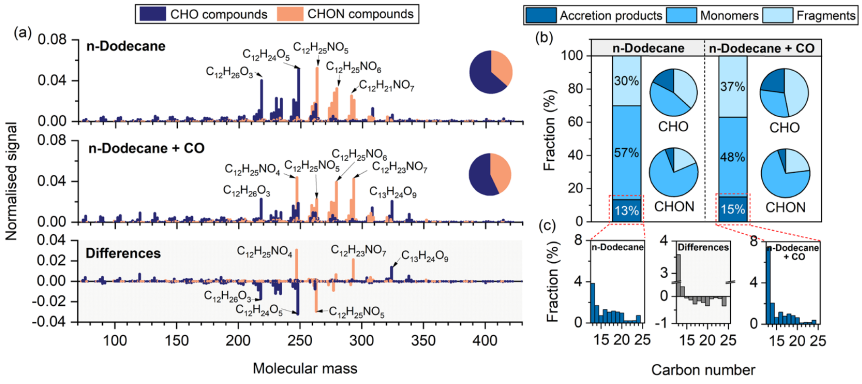

Figure 3: (a) High-resolution mass spectra of particle-phase compounds identified by FIGAERO-CIMS in n-dodecane experiments conducted with and without CO, along with their differences (with CO minus without CO). All signal intensities are normalised to 1. Pie charts display the proportions of CHO and CHON compounds. (b) Fractions of n-dodecane-derived fragments, monomers, and accretion products in the absence and presence of CO. Bar charts represent their contributions to the total signal, while pie charts show their relative contributions within CHO and CHON compounds. (c) Carbon number distributions of accretion products in the absence (left) and presence (right) of CO. The middle panel shows the differences between them (with CO minus without CO).

Compared to α-pinene, the particle-phase products derived from n-dodecane had generally higher molecular mass distributions, mainly within the range of 210 to 310 Da (Fig. 3a). CHON compounds accounted for 37 % and 43 % of the total signal in the absence and presence of CO, respectively. In the absence of CO, the most abundant compounds were $C_{12}H_{25}NO_5$, $C_{12}H_{24}O_5$, and $C_{12}H_{26}O_3$, whereas in the presence of CO, $C_{12}H_{25}NO_4$, $C_{12}H_{23}NO_7$, and $C_{12}H_{25}NO_3$ dominated.

In the n-dodecane systems, compounds containing 12 carbon atoms were classified as monomers, those with fewer than 12 as fragments, and those with more than 12 as accretion products (Fig. 3b). Monomers dominated under both conditions, accounting for 57 % of the total signal in the absence of CO and 48 % in its presence. Differences in carbon number distribution between the two systems were primarily observed in the monomer group (Fig. S10), with CO leading to a lower proportion of C_{12} CHO compounds (e.g., $C_{12}H_{24}O_5$ and $C_{12}H_{26}O_3$) and higher proportion of C_{12} CHON compounds (e.g., $C_{12}H_{25}NO_4$ and $C_{12}H_{23}NO_7$) compared the experiment without CO (Fig. 3a). A few exceptions were observed. For example, an increased contribution from a series of highly oxygenated C_{13} CHO compounds, such as $C_{13}H_{24}O_9$ and $C_{13}H_{22}O_{10}$, was detected in the presence of CO. In contrast, $C_{12}H_{25}NO_5$ showed a higher abundance in the absence of CO. While the overall contribution of accretion products was comparable between two systems, the presence of CO led to a reduced fraction of accretion products containing 16 - 24 carbon atoms compared to experiments without CO (Fig. 3c).

The hydrogen atom number distribution of n-dodecane-derived CHO compounds displayed two peaks at

https://doi.org/10.5194/egusphere-2025-4841
Preprint. Discussion started: 17 October 2025

12 and 24 hydrogen atoms, likely corresponding to fragments and monomers products, respectively (Fig. S11). In the presence of CO, the relative abundance of CHO compounds containing 22, 24, and 26 hydrogen atoms were lower than those observed in the absence of CO. For the identified CHON species, compounds containing 25 hydrogen atoms were the most abundant. The presence of CO led to a general increase in the relative abundances of CHON compounds across the hydrogen atom numbers observed in this study.

3.3 Mixture

3.3.1 SOA particle mass formation and yields

During the first hour of the reaction, O_3 concentrations were comparable between the two systems (Fig. 1a). Thereafter, the CO-present system exhibited higher O_3 levels than the CO-absent system. In both cases, O_3 concentrations peaked during the final hour of the reaction, reaching 81.1 ppb without CO and 101.6 ppb with CO.

The initial precursor/NO_x ratio was 0.8 ± 0.2 (Table 1). NO_x concentrations declined steadily under both conditions throughout the reaction (Fig. S4). In the mixture, the presence of CO led to slower decay rates for both α-pinene and n-dodecane compared to the experiment without CO (Fig. 1d). Nevertheless, α-pinene was fully consumed within three hours in both cases. By the end of the experiment, 25 % of the initial n-dodecane remained unreacted in the absence of CO, whereas 51 % remained when CO was present.

In the absence of CO, 63.9 μg m^{-3} of SOA particles were produced, corresponding to a mass yield of 0.11 (exp. 9). In the presence of CO, 58.8 μg m^{-3} of SOA particles were formed, with a yield of 0.16.

3.3.2 SOA particle chemical composition

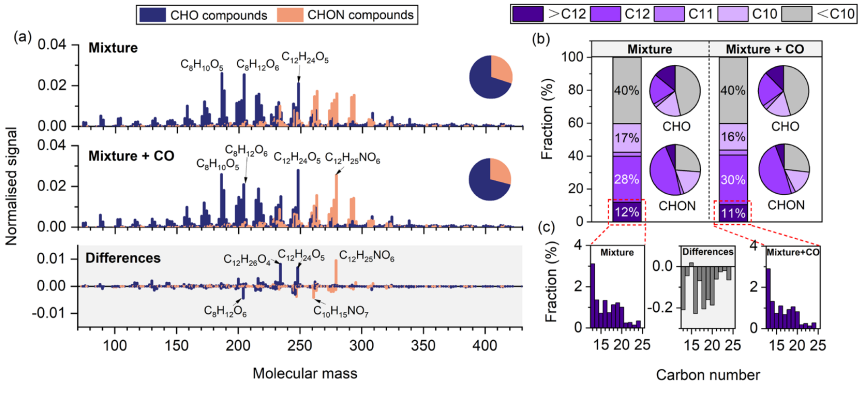

Figure 4: (a) High-resolution mass spectra of particle-phase compounds identified by FIGAERO-CIMS in mixture experiments conducted with and without CO, along with their differences (with CO minus without CO). All signal intensities are normalised to 1. Pie charts display the proportions of CHO and CHON compounds. (b) Fractions of particle-phase products with different carbon numbers in the absence and presence of CO. Bar charts represent their contributions to the total

https://doi.org/10.5194/egusphere-2025-4841
Preprint. Discussion started: 17 October 2025

signal, while pie charts show their relative contributions within CHO and CHON compounds. (c) Carbon number distributions of products with more than 12 carbon atoms in the absence (left) and presence (right) of CO. The middle panel shows the differences between them (with CO minus without CO).

Compared to single-precursor systems, the mixed-precursor system exhibited a broader mass distribution, mainly ranging from 150 to 330 Da (Fig. 4a). CHON compounds accounted for 30 % and 29 % of the total signal in the absence and presence of CO, respectively. In the absence of CO, $C_8H_{10}O_5$, $C_8H_{12}O_6$, and $C_{12}H_{24}O_5$ had the highest signal intensities, whereas in the presence of CO, the most abundant compounds were $C_{12}H_{24}O_5$, $C_8H_{10}NO_5$, and $C_{12}H_{25}NO_6$.

In the mixture, the complexity of interactions made it difficult to clearly distinguish monomers, fragments, and accretion products. Nevertheless, compounds with fewer than 10 carbon atoms were reasonably classified as fragments, while those containing more than 12 carbon atoms were considered accretion products. As shown in Fig. S10, the effect of CO on the carbon distribution in the mixture was generally less pronounced than in the single-precursor systems. While the relative abundances of C10, C12, and accretion products ($C>12$) were similar under both conditions (Fig 4b), small shifts in composition were evident in the presence of CO, displaying features distinct from those in the single-precursor systems. Specifically, CO led to (i) a slightly lower fraction of accretion products containing 13 to 24 carbon atoms (excluding C_{15}) (Fig. 4c), (ii) an increased proportion of C_{12} CHO compounds (e.g., $C_{12}H_{26}O_4$ and $C_{12}H_{24}O_5$), and (iii) a reduced proportion of C_{10} CHON compounds (e.g., $C_{10}H_{15}NO_7$) (Fig. 4a).

As shown in Fig. S11, the hydrogen atom number distribution of mixture-derived CHO compounds showed two peaks at 14 and 24 hydrogen atoms, with the peak at 14 being the most abundant. In the presence of CO, the relative abundances of CHO compounds with 12 and 14 hydrogen atoms decreased, while those with 16, 24, and 26 hydrogen atoms increased. Among the identified CHON species, the presence of CO resulted in an increased fraction of 25-hydrogen compounds and a decreased fraction of 15-hydrogen compounds.

https://doi.org/10.5194/egusphere-2025-4841
Preprint. Discussion started: 17 October 2025

4 Discussion

4.1 Photochemistry

The photochemical reactions in this study involved the presence of NO_x and CO, multiple oxidants (OH and O_3), as well as multiple precursor species. The interactions among these factors substantially increased the complexity of the system, making it challenging to establish experimental conditions that allow for a comparison across different precursor systems. To address this, two key approaches were adopted: (i) ensuring iso-reactivity towards OH radicals, and (ii) maintaining comparable initial precursor/NO_x ratios across systems. Additionally, an oxidant closure approach was employed to characterise the photochemical conditions. As OH radicals could not be measured directly in this study, their concentrations were estimated from the evolution of O_3 and the consumption of precursors, or alternatively, from the depletion of CO. This enabled a quantitative evaluation of the relative contributions of different oxidants to precursor oxidation.

This study was designed for OH radicals to serve as the predominant photochemical loss of precursors. Under iso-reactivity conditions, all systems exhibited comparable initial OH reactivity, and in the mixture experiments, each precursor molecule initially had an equal probability of reacting with OH. However, as the reaction progressed, O_3 gradually accumulated and became increasingly important for the oxidation of O_3-reacting precursors, resulting in the coexistence of two oxidants in the system. Due to the differing reactivities of individual precursors towards O_3, their decay rates varied accordingly (Fig. 1c-d). In the experiments without CO, approximately 70 % of α-pinene decay was attributed to OH oxidation, while the remaining 30 % was driven by ozonolysis (Fig. S12). OH dominated during the early stage of the reaction, contributing over 90 % to α-pinene consumption. However, as the reaction proceeded, the contribution of O_3 became increasingly significant, accounting for over 40 % in the mixture. In contrast, n-dodecane does not react with O_3 and was oxidised exclusively via OH radicals. Thus, although OH remained the dominant oxidant for α-pinene oxidation, the contribution from ozonolysis was still non-negligible.

Owing to the chemical coupling among O_3, NO_x, and RO_x (= OH + RO_2 + HO_2), NO_x plays a critical role in determining both the oxidation conditions and the fate of RO_2 radicals, thereby influencing the yields and chemical composition of SOA particles (Atkinson, 2000; Chen et al., 2022; Clapp and Jenkin, 2001). In this study, NO_x served as the source of OH via O_3 photolysis. The initial precursor/NO_x ratios were maintained at similar levels among different systems, which aimed to minimise systematic discrepancies arising from variations in reaction pathways and thus enabled a more reliable assessment of the effects of CO. Estimated OH levels were largely comparable across systems in the absence of CO (Fig. S5). During the first hour of reaction, O_3 concentrations were also similar, but subsequently both their levels and temporal profiles diverged, leading to differences in overall oxidant levels. In the α-pinene system, O_3 concentrations peaked after approximately two hours of reaction and subsequently declined, while NO_x levels stabilised (Fig. 1a and S4). At this point, over 80 % of α-pinene had been consumed, and the SOA particle formation rate also began to decline (Fig 1b-c). These trends may indicate a diminished rate of RO_2 + NO reactions. The reduced RO_2 + NO reactivity slowed the depletion of NO, which in turn enhanced the titration of O_3 and led to a net O_3 loss. In contrast, in the n-dodecane and mixture systems, over 50 % of n-dodecane was still unreacted after two hours of reaction, and the SOA particle formation rate continued to increase (Fig. 1b-d), indicating that the RO_2 + NO pathway remained active. This

https://doi.org/10.5194/egusphere-2025-4841
Preprint. Discussion started: 17 October 2025

sustained reactivity enabled continuous NO consumption, which in turn limited O_3 titration and let to a net accumulation of O_3.

These results raise an important consideration for studies involving multiple precursors and oxidants. Even when the initial OH reactivity and precursor/NO_x ratios are controlled, differences in precursor reactivities and the close coupling between secondary oxidant formation and precursor oxidation make it challenging to maintain comparable chemical regimes across such systems. As the coexistence of multiple precursors and oxidants is a common feature of the ambient atmosphere, future chamber studies should investigate a broader range of precursor/NO_x ratios and assess the effects of varying oxidants to improve our understanding of SOA formation under atmospherically relevant oxidative conditions.

The addition of CO further perturbed the photochemical processes, altering both oxidant levels and precursor decay rates. Previous studies have demonstrated that CO can suppress SOA particle formation through two main factors: (i) competition with precursors for OH, which is referred to as oxidant (OH) scavenging, and (ii) an elevated HO_2/RO_2 ratio, which favoured $RO_2 + HO_2$ termination pathways rather than $RO_2 + RO_2$ reactions, thereby reducing the formation of accretion products, known as the product scavenging (McFiggans et al., 2019). At the initial stage of the reaction, CO reduced the OH concentrations by approximately 50 % to around 1.5×10^6 molecules cm^{-3} (Fig. S5). However, as the reaction progressed, OH levels gradually recovered and eventually reached values comparable to those observed in the absence of CO. In the presence of CO, both the α-pinene and mixture systems exhibited higher peak O_3 concentrations, whereas in the n-dodecane system O_3 concentrations were generally lower. As shown in Fig 1c-d, CO influenced the decay rates of α-pinene and n-dodecane to different extents. In the α-pinene system, although the α-pinene decay rate was reduced in the presence of CO, the total consumption remained unchanged, and the relative contributions of OH and O_3 showed little variation (Fig. S12). These results suggest that the effect of OH scavenging on the decay of α-pinene was limited. For n-dodecane, OH scavenging had a pronounced effect on its decay, with CO significantly reducing both the consumption rate and overall consumption (Fig. 1c-d).

4.2 Effect of CO on SOA particle mass yields

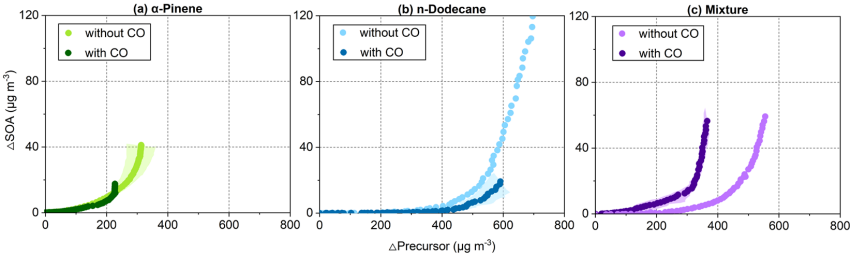

Figure 5: Growth curves of SOA particles formed from (a) α-pinene, (b) n-dodecane, and (c) mixture experiments, defined as the ratio of the mass concentrations of formed SOA particles to the reacted mass of precursors. Shaded areas represent the envelope from repeated experiments.

The influence of CO on SOA particle mass yields differed significantly between the single-precursor and

https://doi.org/10.5194/egusphere-2025-4841
Preprint. Discussion started: 17 October 2025

mixture systems. In the single-precursor systems, CO consistently suppressed the yields, with the effect being more pronounced for n-dodecane than for α-pinene. In the presence of CO, SOA particle mass concentration and yield decreased by 83 % and 79 % for n-dodecane, and by 57 % and 43 % for α-pinene, respectively. One possible factor contributing to this difference is that OH scavenging effect was stronger in the n-dodecane than in the α-pinene system. By contrast, in the mixture, even though OH scavenging was evident, the presence of CO led to only an 8 % decrease in SOA particle mass concentration, whereas the final mass yield showed an increase. To better understand this observation, it may be necessary to distinguish the respective contributions of OH scavenging and product scavenging to the overall effects of CO on yields. Future relevant studies should therefore consider compensating for OH loss to clarify the individual roles of these two scavenging processes (Baker et al., 2024).

Fig. 5 presents the SOA particle growth curves for each system. The induction period is defined as the amount of precursor consumed before SOA particle formation begins (Zhou et al., 2019). Compared with α-pinene, n-dodecane systems had a longer induction period, with the mixture falling in between. In the presence of CO, the induction period was extended in n-dodecane system but remained largely unchanged in the α-pinene system. Notably, the induction period in the mixture system was shortened in the presence of CO. This phenomenon suggests a distinct influence of CO on the SOA formation pathways in the mixed-precursor system compared with the single-precursor systems, as will be discussed in the following section.

4.3 Effect of CO on SOA particle chemical composition

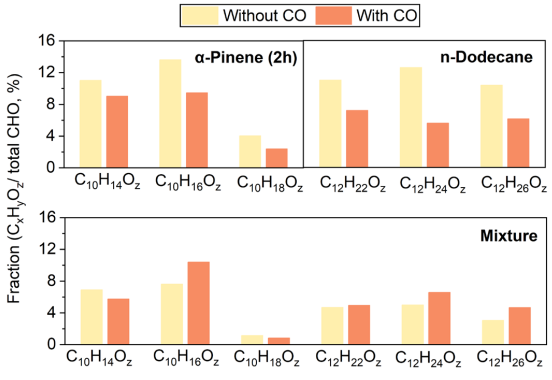

Figure 6: Relative contributions of $C_{10}H_{14}O_Z$, $C_{10}H_{16}O_Z$, $C_{10}H_{18}O_Z$, $C_{12}H_{22}O_Z$, $C_{12}H_{24}O_Z$, and $C_{12}H_{26}O_Z$ to the total CHO compounds in the α-pinene, n-dodecane, and mixture systems in the absence and presence of CO.

4.3.1 Single-precursor systems

The presence of CO led to several consistent changes in the chemical composition of SOA particles in

https://doi.org/10.5194/egusphere-2025-4841
Preprint. Discussion started: 17 October 2025

both the α-pinene and n-dodecane systems, including an increased contribution of CHON compounds, a reduced fraction of C_{16} to C_{24} accretion products, and shifts in the distribution of hydrogen atom numbers. These observations provide evidence for a similar alteration in RO_2 fate in the presence of CO for both systems.

CHON compounds constituted a significant fraction of the SOA particles, indicating that reactions with NO were also an important RO_2 termination pathway in our experiments. In the presence of CO, the increase in total CHON fractions in both α-pinene and n-dodecane systems was mainly attributed to enhanced contributions from specific C_{10} and C_{12} CHON compounds, respectively (Fig. S10). These findings suggest that the suppression of RO_2 + RO_2 termination pathways induced by CO may have increased the relative importance of monomer-derived RO_2 + NO reactions.

The presence of CO did not significantly alter the overall contribution of accretion products to the SOA particles in the single-precursor systems. However, the contribution of those containing 16 to 24 carbon atoms decreased in both systems (Fig. 2c and 3c). Correspondingly, in the α-pinene system, the relative abundance of accretion products with 11 to 15 carbon atoms increased, while in the n-dodecane system, those with 13 to 14 carbon atoms became more abundant. Accretion products are typically formed via the chemical bonding of two RO_2 radicals (Berndt et al., 2018). Compounds with fewer carbon atoms are likely derived from reactions involving fragment-derived RO_2 radicals, whereas those with higher carbon numbers are more likely formed through reactions between monomer-derived RO_2 radicals and fragment-derived RO_2 radicals, or between two monomer-derived RO_2 radicals (Berndt et al., 2018). An elevated HO_2/RO_2 ratio can suppress RO_2 + RO_2 pathway, thereby altering the product distribution. Previous studies have quantitatively assessed the effect of CO on the chemical composition of SOA from α-pinene, reporting a twofold reduction in C_{17} to C_{20} HOM dimers (McFiggans et al., 2019). After compensating for the OH consumption by CO, α-pinene-derived HOM accretion products were reduced by approximately 60% under CO-present conditions (Baker et al., 2024). In this study, quantitative assessment of accretion product concentrations was not possible due to instrumental limitations. Nevertheless, based on the changes in the relative contributions of accretion products and the SOA particle mass concentration, it can be inferred that the suppression effect of CO on RO_2 + RO_2 reactions was more pronounced for monomer-derived RO_2 radicals than for fragment-derived ones.

The shifts in hydrogen atom distributions further supported the above interpretation of altered RO_2 termination pathways under CO-present conditions. Fig. S11 presents the distribution of hydrogen atom numbers across different systems. Similar patterns were observed in both the α-pinene and n-dodecane systems. In the α-pinene system, the presence of CO led to a decrease in the relative abundance of CHO compounds containing 14, 16, and 18 hydrogen atoms. Specifically, the relative contributions of $C_{10}H_{14}O_z$, $C_{10}H_{16}O_z$, and $C_{10}H_{18}O_z$ species to CHO compounds were reduced by 2.0 %, 4.2 %, and 1.6 %, respectively, in the presence of CO (Fig. 6). The main RO_2 radicals generated from α-pinene photooxidation are $C_{10}H_{15}O_x$ and $C_{10}H_{17}O_x$ (Baker et al., 2024). HO_2 termination of $C_{10}H_{15}O_x$ radicals forms multifunctional hydroperoxides ($C_{10}H_{16}O_z$), whereas RO_2 termination produce $C_{10}H_{14}O_z$ carbonyls and $C_{10}H_{16}O_z$ alcohols. Similarly, HO_2 termination of $C_{10}H_{17}O_x$ radicals form $C_{10}H_{18}O_z$ hydroperoxides, and RO_2 termination yield $C_{10}H_{16}O_z$ carbonyls and $C_{10}H_{18}O_z$ alcohols. Cross-reactions between $C_{10}H_{15}O_x$ and $C_{10}H_{17}O_x$ radicals lead to the formation of $C_{10}H_{14}O_z$ carbonyls and $C_{10}H_{18}O_z$ alcohols, and/or $C_{10}H_{16}O_z$ carbonyls and alcohols. Therefore, while $C_{10}H_{16}O_z$ and $C_{10}H_{18}O_z$ species can be produced

https://doi.org/10.5194/egusphere-2025-4841
Preprint. Discussion started: 17 October 2025

through multiple termination pathways, the formation of $C_{10}H_{14}O_z$ occurs exclusively via RO_2 + RO_2 reactions. For n-dodecane, the presence of CO led to a decrease in the relative abundance of CHO compounds containing 22, 24, and 26 hydrogen atoms. Specifically, the relative contributions of $C_{12}H_{22}O_z$, $C_{12}H_{24}O_z$, and $C_{12}H_{26}O_z$ species decreased by 3.8 %, 7.0 %, and 4.2 %, respectively, in the presence of CO (Fig. 6). The discussion here focuses primarily on the $C_{12}H_{24}O_z$, and $C_{12}H_{26}O_z$ families. The main RO_2 radicals generated from n-dodecane photooxidation is $C_{12}H_{25}O_x$ (Zhang et al., 2014). HO_2 termination yields $C_{12}H_{26}O_z$ hydroperoxides, while RO_2 termination produce $C_{12}H_{24}O_z$ carbonyls and $C_{12}H_{26}O_z$ alcohols. The $C_{12}H_{24}O_z$ family is formed exclusively through RO_2 + RO_2 reactions. The reductions in the relative abundances of $C_{10}H_{14}O_z$ and $C_{12}H_{24}O_z$ in the α-pinene and n-dodecane systems, respectively, thus provide further evidence that the presence of CO suppressed the RO_2 + RO_2 reaction pathway.

4.3.2 Mixed-precursor system

Compared with the single-precursor systems, the influence of CO on the chemical composition of SOA in the mixed-precursor system was different: (i) the addition of CO did not significantly alter the proportion of CHON compounds, indicating that the relative importance of the RO_2 + NO pathway remained largely unchanged; (ii) the relative contributions of C_{13} to C_{24} accretion products (excluding C_{15}) slightly decreased, indicating a moderate suppression of the RO_2 + RO_2 pathway; (iii) the changes in hydrogen atom distributions differed from those observed in the single-precursor systems, possibly implying a distinct influence on the RO_2 reaction pathways.

In the mixed-precursor system, RO_2 termination reactions were expected to be more complex than those in single-precursor systems. In addition to the pathways discussed above, cross-reactions between RO_2 radicals originating from different precursors may also occur. RO_2 + RO_2 reactions between $C_{10}H_{15}O_x$ and $C_{12}H_{25}O_x$ yield $C_{10}H_{14}O_z$ carbonyls and $C_{12}H_{26}O_z$ alcohols or $C_{12}H_{24}O_z$ carbonyls and $C_{10}H_{16}O_z$ alcohols. Similarly, reactions between $C_{10}H_{17}O_x$ and $C_{12}H_{25}O_x$ lead to the formation of $C_{10}H_{16}O_z$ carbonyls and $C_{12}H_{26}O_z$ alcohols, or $C_{12}H_{24}O_z$ carbonyls and $C_{10}H_{18}O_z$ alcohols. In the mixture, the presence of CO led to a decrease in the relative contributions of $C_{10}H_{14}O_z$ and $C_{10}H_{18}O_z$ families by 1.2 % and 0.3 %, respectively, while the relative contributions of $C_{10}H_{16}O_z$, $C_{12}H_{24}O_z$, and $C_{12}H_{26}O_z$ families increased by 2.8 %, 1.6 %, and 1.6 %, respectively (Fig. 6). Based on the carbon number distributions observed in the single-precursor systems, it was reasonably assumed that C_{10} compounds in the mixture primarily originated from α-pinene, while C_{12} compounds were mainly derived from n-dodecane. The decrease in the fraction of the $C_{10}H_{14}O_z$ family suggests that, in the presence of CO, the relative abundance of the RO_2 termination involving a-pinene-derived RO_2 and/or cross-reactions between $C_{10}H_{15}O_x$ and $C_{12}H_{25}O_x$ became less pronounced in the mixture. In contrast, the relative abundance of $C_{12}H_{24}O_z$ family increased in the mixture in the presence of CO. Taken together with the observed increase in the contribution of C_{12} species and decrease in C_{10} species in the mixture (Fig. S10), this suggest that CO exerted a weaker suppression effect on cross-reactions involving n-dodecane-derived RO_2 than on those involving α-pinene-derived RO_2. However, due to the lack of quantitative measurements on individual accretion products, the extent of this effect remains unclear. Moreover, as α-pinene and n-dodecane were used as representative precursors, the findings may be specific to the present system. These uncertainties highlight the need for future chamber studies to investigate a broader range of precursor combinations to assess the generality of the observed behaviour.

https://doi.org/10.5194/egusphere-2025-4841
Preprint. Discussion started: 17 October 2025

5 Implications

We established a photochemical system in the MAC that incorporated both biogenic and anthropogenic precursors, together with coexisting CO and NO_x. Compared to the chamber studies conducted under simplified conditions, this setup is more representative of polluted atmospheric environments, enabling a better characterisation of real-world SOA formation processes. Our findings show that, under altered reaction conditions, the changes in SOA particle mass yields and chemical composition differed markedly between single- and mixed-precursor systems.

Although biogenic precursors contribute more substantially to SOA formation on a global scale, anthropogenic precursors can play a significant role in urban and suburban environments (Srivastava et al., 2022; Stone et al., 2010; Volkamer et al., 2006). Such regions are often characterised by elevated levels of other pollutants with strong anthropogenic sources, such as CO and NO_x, which can alter oxidant budgets and shift radical reaction pathways. Consequently, model parameterisations derived under single-precursor or idealised conditions may misrepresent SOA formation in non-clean environments. Future laboratory studies should simulate the chemical complexity of the real atmosphere by incorporating representative precursor mixture and common trace gases, thereby providing a more reliable basis for the development of accurate SOA model parameterisations.

In this study, the initial experimental conditions were designed to maintain comparable precursor/NO_x ratios and iso-reactivity towards OH across systems. However, results showed that variations in oxidant levels still led to differences in precursor decay rates and potentially the SOA formation. This highlights the need for carefully defining comparable reaction conditions across parallel experiments involving complex photochemical systems where multiple precursors and oxidants coexist. Future work should systematically investigate SOA formation under controlled variations in oxidant levels and precursor/NO_x ratios to improve the reliability and comparability of experimental results.

6 Conclusions

This study investigated the impact of CO on SOA particle mass yields and chemical composition from a biogenic VOC (α-pinene), an anthropogenic IVOC (n-dodecane), and their mixture in the presence of NO_x. The results indicate that the effects differed between the single- and mixed-precursor systems.

In the single-precursor systems, the presence of CO led to a notable reduction in SOA particle mass yields, with the suppression being more pronounced for n-dodecane than for α-pinene. By contrast, no such suppression was observed in the mixture.

Chemical composition analysis revealed consistent trends in the single-precursor systems, indicating similar shifts in RO_2 termination pathways. In both α-pinene and n-dodecane single-precursor systems, the presence of CO increased the relative abundance of CHON species and decreased the fraction of C_{16} to C_{24} accretion products. The α-pinene system showed a reduction in the fraction of the $C_{10}H_{14}O_z$ family, while the n-dodecane system exhibited a decrease in the fraction of $C_{12}H_{24}O_z$ family. These findings suggest that the RO_2 + RO_2 pathway was suppressed under CO-present conditions. In the mixed-precursor systems, the reduction in the fraction of C_{16} to C_{24} accretion products was more moderate, and

https://doi.org/10.5194/egusphere-2025-4841
Preprint. Discussion started: 17 October 2025

the contribution of CHON species remained largely unchanged. The fraction of $C_{10}H_{14}O_z$ family decreased, whereas the $C_{12}H_{24}O_z$ family increased. These contrasting changes may suggest that CO suppressed the two precursors to different extents in the mixture, with its influence on n-dodecane being less pronounced than in the single-precursor system, thereby resulting in a relatively small overall impact of CO in the mixture.

These results demonstrate that variations in reaction conditions led to different responses in SOA particle mass yields and composition between the single- and mixed-precursor systems, highlighting the need for laboratory experiments conducted under atmospherically relevant conditions.

Data availability

All the data in the figures of this study are available upon request to the corresponding authors (g.mcfiggans@manchester.ac.uk and aristeidis.voliotis@manchester.ac.uk)

Author contribution

GX, AV, and GM conceived the study. GX and AV conducted the experiments. AV, TJB, YS, HW, DH provided assistance in instrument operation and data analysis. GX conducted the data analysis and wrote the manuscript with inputs from all the co-authors.

Competing interests

The contact author has declared that none of the authors has any competing interests.

Acknowledgements

Guangzhao Xie acknowledges the joint scholarship of The University of Manchester and Chinese Scholarship Council (CSC) (grant no. 202208330060). Gordon McFiggans acknowledges funding from the Secondary Organic Aerosol Prediction in Realistic Atmospheres (SOAPRA) project (grant no. NE/V012665/1). Aristeidis Voliotis acknowledges funding support from the Natural Environment Research Council (NERC) through the UK National Centre for Atmospheric Science (NCAS). We thank colleagues from the Jülich and Gothenburg teams for valuable discussions, especially Thomas F. Mentel, Mattias Hallquist, and Sören R. Zorn. We acknowledge the use of ChatGPT (https://chatgpt.com/) for assistance in language refinement of this manuscript.

https://doi.org/10.5194/egusphere-2025-4841
Preprint. Discussion started: 17 October 2025

References

Amedro, D., Miyazaki, K., Parker, A., Schoernaecker, C. and Fittschen, C.: Atmospheric and kinetic studies of OH and HO2 by the FAGE technique, J. Environ. Sci., 24, 78-86, http://doi.org/10.1016/s1001-0742(11)60723-7, 2012.

Andreae, M.O. and Crutzen, P.J.: Atmospheric aerosols: biogeochemical sources and role in atmospheric chemistry, Science, 276, 1052-1058, http://doi.org/10.1126/science.276.5315.1052, 1997.

Atkinson, R.: Atmospheric chemistry of VOCs and NOx, Atmos. Environ., 34, 2063-2101, http://doi.org/10.1016/s1352-2310(99)00460-4, 2000.

Atkinson, R.: Kinetics of the gas-phase reactions of OH radicals with alkanes and cycloalkanes, Atmos. Chem. Phys., 3, 2233-2307, http://doi.org/10.5194/acp-3-2233-2003, 2003.

Atkinson, R. and Arey, J.: Atmospheric degradation of volatile organic compounds, Chem. Rev., 103, 4605-4638, http://doi.org/10.1021/cr0206420, 2003.

Baker, Y., Kang, S., Wang, H., Wu, R.R., Xu, J., Zanders, A., He, Q.F., Hohaus, T., Ziehm, T., Geretti, V., Bannan, T.J., O'Meara, S.P., Voliotis, A., Hallquist, M., McFiggans, G., Zorn, S.R., Wahner, A. and Mentel, T.F.: Impact of HO2/RO2 ratio on highly oxygenated α-pinene photooxidation products and secondary organic aerosol formation potential, Atmos. Chem. Phys., 24, 4789-4807, http://doi.org/10.5194/acp-24-4789-2024, 2024.

Baltensperger, U., Kalberer, M., Dommen, J., Paulsen, D., Alfarra, M.R., Coe, H., Fisseha, R., Gascho, A., Gysel, M., Nyeki, S., Sax, M., Steinbacher, M., Prevot, A.S.H., Sjogren, S., Weingartner, E. and Zenobi, R.: Secondary organic aerosols from anthropogenic and biogenic precursors, Faraday Discuss., 130, 265-278, http://doi.org/10.1039/b417367h, 2005.

Bannan, T.J., Le Breton, M., Priestley, M., Worrall, S.D., Bacak, A., Marsden, N.A., Mehra, A., Hammes, J., Hallquist, M., Alfarra, M.R., Krieger, U.K., Reid, J.P., Jayne, J., Robinson, W., McFiggans, G., Coe, H., Percival, C.J. and Topping, D.: A method for extracting calibrated volatility information from the FIGAERO-HR-ToF-CIMS and its experimental application, Atmos. Meas. Tech., 12, 1429-1439, http://doi.org/10.5194/amt-12-1429-2019, 2019.

Berndt, T., Mentler, B., Scholz, W., Fischer, L., Herrmann, H., Kulmala, M. and Hansel, A.: Accretion product formation from ozonolysis and OH radical reaction of α-pinene: Mechanistic insight and the influence of isoprene and ethylene, Environ. Sci. Technol., 52, 11069-11077, http://doi.org/10.1021/acs.est.8b02210, 2018.

Burkholder, J.B., Abbatt, J.P.D., Barnes, I., Roberts, J.M., Melamed, M.L., Ammann, M., Bertram, A.K., Cappa, C.D., Carlton, A.G., Carpenter, L.J., Crowley, J.N., Dubowski, Y., Georges, C., Heard, D.E., Herrmann, H., Keutsch, F.N., Kroll, J.H., McNeill, V.F., Ng, N.L., Nizkorodov, S.A., Orlando, J.J., Percival, C.J., Picquet-Varrault, B., Rudich, Y., Seakins, P.W., Surratt, J.D., Tanimoto, H., Thornton, J.A., Tong, Z., Tyndall, G.S., Wahner, A., Weschler, C.J., Wilson, K.R. and Ziemann, P.J.: The essential role for laboratory studies in atmospheric chemistry, Environ. Sci. Technol., 51, 2519-2528, http://doi.org/10.1021/acs.est.6b04947, 2017.

Chen, T.Z., Zhang, P., Ma, Q.X., Chu, B.W., Liu, J., Ge, Y.L. and He, H.: Smog chamber study on the role of NOx in SOA and O3 formation from aromatic hydrocarbons, Environ. Sci. Technol., http://doi.org/10.1021/acs.est.2c04022, 2022.

Clapp, L.J. and Jenkin, M.E.: Analysis of the relationship between ambient levels Of O3, NO2 and NO as a function of NOχ in the UK, Atmos. Environ., 35, 6391-6405, http://doi.org/10.1016/s1352-2310(01)00378-8, 2001.

Dash, M.R., Balaganesh, M. and Rajakumar, B.: Rate coefficients for the gas-phase reaction of OH

https://doi.org/10.5194/egusphere-2025-4841
Preprint. Discussion started: 17 October 2025

radical with α-pinene: an experimental and computational study, Mol. Phys., 112, 1495-1511, http://doi.org/10.1080/00268976.2013.840395, 2014.

Drewnick, F., Hings, S.S., Alfarra, M.R., Prevot, A.S.H. and Borrmann, S.: Aerosol quantification with the Aerodyne Aerosol Mass Spectrometer: detection limits and ionizer background effects, Atmos. Meas. Tech., 2, 33-46, http://doi.org/10.5194/amt-2-33-2009, 2009.

Gao, L.Y., Song, J.W., Mohr, C., Huang, W., Vallon, M., Jiang, F., Leisner, T. and Saathoff, H.: Kinetics, SOA yields, and chemical composition of seconaary organic aerosol from β-caryophyllene ozonolysis with and without nitrogen oxides between 213 and 313 K, Atmos. Chem. Phys., 22, 6001-6020, http://doi.org/10.5194/acp-22-6001-2022, 2022.

Gu, S., Guenther, A. and Faiola, C.: Effects of anthropogenic and biogenic volatile organic compounds on Los Angeles air quality, Environ. Sci. Technol., 55, 12191-12201, http://doi.org/10.1021/acs.est.1c01481, 2021.

Guenther, A., Hewitt, C.N., Erickson, D., Fall, R., Geron, C., Graedel, T., Harley, P., Klinger, L., Lerdau, M., Mckay, W.A., Pierce, T., Scholes, B., Steinbrecher, R., Tallamraju, R., Taylor, J. and Zimmerman, P.: A global model of natural volatile organic compound emissions, J. Geophys. Res., 100, 8873-8892, http://doi.org/https://doi.org/10.1029/94JD02950, 1995.

Hallquist, M., Wenger, J.C., Baltensperger, U., Rudich, Y., Simpson, D., Claeys, M., Dommen, J., Donahue, N.M., George, C., Goldstein, A.H., Hamilton, J.F., Herrmann, H., Hoffmann, T., Iinuma, Y., Jang, M., Jenkin, M.E., Jimenez, J.L., Kiendler-Scharr, A., Maenhaut, W., McFiggans, G., Mentel, T.F., Monod, A., Prevot, A.S.H., Seinfeld, J.H., Surratt, J.D., Szmigielski, R. and Wildt, J.: The formation, properties and impact of secondary organic aerosol: current and emerging issues, Atmos. Chem. Phys., 9, 5155-5236, http://doi.org/10.5194/acp-9-5155-2009, 2009.

Jensen, A.R., Koss, A.R., Hales, R.B. and de Gouw, J.A.: Measurements of volatile organic compounds in ambient air by gas-chromatography and real-time Vocus PTR-TOF-MS: calibrations, instrument background corrections, and introducing a PTR Data Toolkit, Atmos. Meas. Tech., 16, 5261-5285, http://doi.org/10.5194/amt-16-5261-2023, 2023.

Jimenez, J.L., Canagaratna, M.R., Donahue, N.M., Prevot, A.S.H., Zhang, Q., Kroll, J.H., DeCarlo, P.F., Allan, J.D., Coe, H., Ng, N.L., Aiken, A.C., Docherty, K.S., Ulbrich, I.M., Grieshop, A.P., Robinson, A.L., Duplissy, J., Smith, J.D., Wilson, K.R., Lanz, V.A., Hueglin, C., Sun, Y.L., Tian, J., Laaksonen, A., Raatikainen, T., Rautiainen, J., Vaattovaara, P., Ehn, M., Kulmala, M., Tomlinson, J.M., Collins, D.R., Cubison, M.J., Dunlea, E.J., Huffman, J.A., Onasch, T.B., Alfarra, M.R., Williams, P.I., Bower, K., Kondo, Y., Schneider, J., Drewnick, F., Borrmann, S., Weimer, S., Demerjian, K., Salcedo, D., Cottrell, L., Griffin, R., Takami, A., Miyoshi, T., Hatakeyama, S., Shimono, A., Sun, J.Y., Zhang, Y.M., Dzepina, K., Kimmel, J.R., Sueper, D., Jayne, J.T., Herndon, S.C., Trimborn, A.M., Williams, L.R., Wood, E.C., Middlebrook, A.M., Kolb, C.E., Baltensperger, U. and Worsnop, D.R.: Evolution of Organic Aerosols in the Atmosphere, Science, 326, 1525-1529, http://doi.org/10.1126/science.1180353, 2009.

Kanakidou, M., Seinfeld, J.H., Pandis, S.N., Barnes, I., Dentener, F.J., Facchini, M.C., Van Dingenen, R., Ervens, B., Nenes, A., Nielsen, C.J., Swietlicki, E., Putaud, J.P., Balkanski, Y., Fuzzi, S., Horth, J., Moortgat, G.K., Winterhalter, R., Myhre, C.E.L., Tsigaridis, K., Vignati, E., Stephanou, E.G. and Wilson, J.: Organic aerosol and global climate modelling: a review, Atmos. Chem. Phys., 5, 1053-1123, http://doi.org/10.5194/acp-5-1053-2005, 2005.

Kang, S., Wildt, J., Pullinen, I., Vereecken, L., Wu, C., Wahner, A., Zorn, S.R. and Mentel, T.F.: Formation of highly oxygenated organic molecules from α-pinene photooxidation: evidence for the importance of highly oxygenated alkoxy radicals, EGUsphere, 2025, 1-33,

https://doi.org/10.5194/egusphere-2025-4841
Preprint. Discussion started: 17 October 2025

http://doi.org/10.5194/egusphere-2025-2772, 2025.

Kenagy, H.S., Heald, C.L., Tahsini, N., Goss, M.B. and Kroll, J.H.: Can we achieve atmospheric chemical environments in the laboratory? An integrated model-measurement approach to chamber SOA studies, 10, eado1482, http://doi.org/doi:10.1126/sciadv.ado1482, 2024.

Krechmer, J., Lopez-Hilfiker, F., Koss, A., Hutterli, M., Stoermer, C., Deming, B., Kimmel, J., Warneke, C., Holzinger, R., Jayne, J., Worsnop, D., Fuhrer, K., Gonin, M. and de Gouw, J.: Evaluation of a new reagent-ion source and focusing Ion-Molecule Reactor for use in Proton-Transfer-Reaction Mass Spectrometry, Anal. Chem., 90, 12011-12018, http://doi.org/10.1021/acs.analchem.8b02641, 2018.

Kroll, J.H. and Seinfeld, J.H.: Chemistry of secondary organic aerosol: Formation and evolution of low-volatility organics in the atmosphere, Atmos. Environ., 42, 3593-3624, http://doi.org/10.1016/j.atmosenv.2008.01.003, 2008.

Lane, T.E., Donahue, N.M. and Pandis, S.N.: Effect of NOx on secondary organic aerosol concentrations, Environ. Sci. Technol., 42, 6022-6027, http://doi.org/10.1021/es703225a, 2008.

Lee, A., Goldstein, A.H., Kroll, J.H., Ng, N.L., Varutbangkul, V., Flagan, R.C. and Seinfeld, J.H.: Gas-phase products and secondary aerosol yields from the photooxidation of 16 different terpenes, J. Geophys. Res. Atmos., 111, http://doi.org/10.1029/2006jd007050, 2006.

Lopez-Hilfiker, F.D., Mohr, C., Ehn, M., Rubach, F., Kleist, E., Wildt, J., Mentel, T.F., Lutz, A., Hallquist, M., Worsnop, D. and Thornton, J.A.: A novel method for online analysis of gas and particle composition: description and evaluation of a Filter Inlet for Gases and AEROsols (FIGAERO), Atmos. Meas. Tech., 7, 983-1001, http://doi.org/10.5194/amt-7-983-2014, 2014.

Lu, Y. and Khalil, M.A.K.: Methane and carbon-monoxide in OH chemistry - The effects of feedbacks and reservoirs generated by the reactive products, Chemosphere, 26, 641-655, http://doi.org/10.1016/0045-6535(93)90450-j, 1993.

McFiggans, G., Mentel, T.F., Wildt, J., Pullinen, I., Kang, S., Kleist, E., Schmitt, S., Springer, M., Tillmann, R., Wu, C., Zhao, D.F., Hallquist, M., Faxon, C., Le Breton, M., Hallquist, A.M., Simpson, D., Bergstrom, R., Jenkin, M.E., Ehn, M., Thornton, J.A., Alfarra, M.R., Bannan, T.J., Percival, C.J., Priestley, M., Topping, D. and Kiendler-Scharr, A.: Secondary organic aerosol reduced by mixture of atmospheric vapours, Nature, 565, 587-593, http://doi.org/10.1038/s41586-018-0871-y, 2019.

Nah, T., McVay, R.C., Pierce, J.R., Seinfeld, J.H. and Ng, N.L.: Constraining uncertainties in particle-wall deposition correction during SOA formation in chamber experiments, Atmos. Chem. Phys., 17, 2297-2310, http://doi.org/10.5194/acp-17-2297-2017, 2017.

Ng, N.L., Chhabra, P.S., Chan, A.W.H., Surratt, J.D., Kroll, J.H., Kwan, A.J., McCabe, D.C., Wennberg, P.O., Sorooshian, A., Murphy, S.M., Dalleska, N.F., Flagan, R.C. and Seinfeld, J.H.: Effect of NOx level on secondary organic aerosol (SOA) formation from the photooxidation of terpenes, Atmos. Chem. Phys., 7, 5159-5174, http://doi.org/10.5194/acp-7-5159-2007, 2007.

Pullinen, I., Schmitt, S., Kang, S., Sarrafzadeh, M., Schlag, P., Andres, S., Kleist, E., Mentel, T.F., Rohrer, F., Springer, M., Tillmann, R., Wildt, J., Wu, C., Zhao, D., Wahner, A. and Kiendler-Scharr, A.: Impact of NOx on secondary organic aerosol (SOA) formation from α-pinene and β-pinene photooxidation: the role of highly oxygenated organic nitrates, Atmos. Chem. Phys., 20, 10125-10147, http://doi.org/10.5194/acp-20-10125-2020, 2020.

Ramanathan, V., Crutzen, P.J., Kiehl, J.T. and Rosenfeld, D.: Atmosphere - Aerosols, climate, and the hydrological cycle, Science, 294, 2119-2124, http://doi.org/10.1126/science.1064034, 2001.

Robinson, A.L., Donahue, N.M., Shrivastava, M.K., Weitkamp, E.A., Sage, A.M., Grieshop, A.P., Lane, T.E., Pierce, J.R. and Pandis, S.N.: Rethinking organic aerosols: Semivolatile emissions and

https://doi.org/10.5194/egusphere-2025-4841
Preprint. Discussion started: 17 October 2025

photochemical aging, Science, 315, 1259-1262, http://doi.org/10.1126/science.1133061, 2007.

Shao, Y.Q., Voliotis, A., Du, M., Wang, Y., Pereira, K., Hamilton, J., Alfarra, M.R. and McFiggans, G.: Chemical composition of secondary organic aerosol particles formed from mixtures of anthropogenic and biogenic precursors, Atmos. Chem. Phys., 22, 9799-9826, http://doi.org/10.5194/acp-22-9799-2022, 2022a.

Shao, Y.Q., Wang, Y., Du, M., Voliotis, A., Alfarra, M.R., O'Meara, S.P., Turner, S.F. and McFiggans, G.: Characterisation of the Manchester Aerosol Chamber facility, Atmos. Meas. Tech., 15, 539-559, http://doi.org/10.5194/amt-15-539-2022, 2022b.

Shilling, J.E., Zaveri, R.A., Fast, J.D., Kleinman, L., Alexander, M.L., Canagaratna, M.R., Fortner, E., Hubbe, J.M., Jayne, J.T., Sedlacek, A., Setyan, A., Springston, S., Worsnop, D.R. and Zhang, Q.: Enhanced SOA formation from mixed anthropogenic and biogenic emissions during the CARES campaign, Atmos. Chem. Phys., 13, 2091-2113, http://doi.org/10.5194/acp-13-2091-2013, 2013.

Shrivastava, M., Cappa, C.D., Fan, J.W., Goldstein, A.H., Guenther, A.B., Jimenez, J.L., Kuang, C., Laskin, A., Martin, S.T., Ng, N.L., Petaja, T., Pierce, J.R., Rasch, P.J., Roldin, P., Seinfeld, J.H., Shilling, J., Smith, J.N., Thornton, J.A., Volkamer, R., Wang, J., Worsnop, D.R., Zaveri, R.A., Zelenyuk, A. and Zhang, Q.: Recent advances in understanding secondary organic aerosol: Implications for global climate forcing, Rev. Geophys., 55, 509-559, http://doi.org/10.1002/2016rg000540, 2017.

Srivastava, D., Vu, T.V., Tong, S., Shi, Z. and Harrison, R.M.: Formation of secondary organic aerosols from anthropogenic precursors in laboratory studies, npj Clim. Atmos. Sci., 5, 22, http://doi.org/10.1038/s41612-022-00238-6, 2022.

Stone, E.A., Hedman, C.J., Zhou, J., Mieritz, M. and Schauer, J.J.: Insights into the nature of secondary organic aerosol in Mexico City during the MILAGRO experiment 2006, Atmos. Environ., 44, 312-319, http://doi.org/https://doi.org/10.1016/j.atmosenv.2009.10.036, 2010.

Takeuchi, M., Berkemeier, T., Eris, G. and Ng, N.L.: Non-linear effects of secondary organic aerosol formation and properties in multi-precursor systems, Nat. Commun., 13, http://doi.org/10.1038/s41467-022-35546-1, 2022.

Tsigaridis, K., Daskalakis, N., Kanakidou, M., Adams, P.J., Artaxo, P., Bahadur, R., Balkanski, Y., Bauer, S.E., Bellouin, N., Benedetti, A., Bergman, T., Berntsen, T.K., Beukes, J.P., Bian, H., Carslaw, K.S., Chin, M., Curci, G., Diehl, T., Easter, R.C., Ghan, S.J., Gong, S.L., Hodzic, A., Hoyle, C.R., Iversen, T., Jathar, S., Jimenez, J.L., Kaiser, J.W., Kirkevåg, A., Koch, D., Kokkola, H., Lee, Y.H., Lin, G., Liu, X., Luo, G., Ma, X., Mann, G.W., Mihalopoulos, N., Morcrette, J.J., Müller, J.F., Myhre, G., Myriokefalitakis, S., Ng, N.L., O'Donnell, D., Penner, J.E., Pozzoli, L., Pringle, K.J., Russell, L.M., Schulz, M., Sciare, J., Seland, O., Shindell, D.T., Sillman, S., Skeie, R.B., Spracklen, D., Stavrakou, T., Steenrod, S.D., Takemura, T., Tiitta, P., Tilmes, S., Tost, H., van Noije, T., van Zyl, P.G., von Salzen, K., Yu, F., Wang, Z., Wang, Z., Zaveri, R.A., Zhang, H., Zhang, K., Zhang, Q. and Zhang, X.: The AeroCom evaluation and intercomparison of organic aerosol in global models, Atmos. Chem. Phys., 14, 10845-10895, http://doi.org/10.5194/acp-14-10845-2014, 2014.

Voliotis, A., Du, M., Wang, Y., Shao, Y.Q., Alfarra, M.R., Bannan, T.J., Hu, D.W., Pereira, K.L., Hamilton, J.F., Hallquist, M., Mentel, T.F. and McFiggans, G.: Chamber investigation of the formation and transformation of secondary organic aerosol in mixtures of biogenic and anthropogenic volatile organic compounds, Atmos. Chem. Phys., 22, 14147-14175, http://doi.org/10.5194/acp-22-14147-2022, 2022a.

Voliotis, A., Du, M., Wang, Y., Shao, Y.Q., Bannan, T.J., Flynn, M., Pandis, S.N., Percival, C.J., Alfarra, M.R. and McFiggans, G.: The influence of the addition of isoprene on the volatility of particles formed from the photo-oxidation of anthropogenic-biogenic mixtures, Atmos. Chem. Phys., 22, 13677-13693,

https://doi.org/10.5194/egusphere-2025-4841
Preprint. Discussion started: 17 October 2025

http://doi.org/10.5194/acp-22-13677-2022, 2022b.

Voliotis, A., Wang, Y., Shao, Y.Q., Du, M., Bannan, T.J., Percival, C.J., Pandis, S.N., Alfarra, M.R. and McFiggans, G.: Exploring the composition and volatility of secondary organic aerosols in mixed anthropogenic and biogenic precursor systems, Atmos. Chem. Phys., 21, 14251-14273, http://doi.org/10.5194/acp-21-14251-2021, 2021.

Volkamer, R., Jimenez, J.L., San Martini, F., Dzepina, K., Zhang, Q., Salcedo, D., Molina, L.T., Worsnop, D.R. and Molina, M.J.: Secondary organic aerosol formation from anthropogenic air pollution: Rapid and higher than expected, 33, http://doi.org/https://doi.org/10.1029/2006GL026899, 2006.

Wang, N.X., Jorga, S.D., Pierce, J.R., Donahue, N.M. and Pandis, S.N.: Particle wall-loss correction methods in smog chamber experiments, Atmos. Meas. Tech., 11, 6577-6588, http://doi.org/10.5194/amt-11-6577-2018, 2018.

Yuan, B., Koss, A.R., Warneke, C., Coggon, M., Sekimoto, K. and de Gouw, J.A.: Proton-Transfer-Reaction Mass Spectrometry: Applications in atmospheric sciences, Chem. Rev., 117, 13187-13229, http://doi.org/10.1021/acs.chemrev.7b00325, 2017.

Zhang, X., Schwantes, R.H., Coggon, M.M., Loza, C.L., Schilling, K.A., Flagan, R.C. and Seinfeld, J.H.: Role of ozone in SOA formation from alkane photooxidation, Atmos. Chem. Phys., 14, 1733-1753, http://doi.org/10.5194/acp-14-1733-2014, 2014.

Zhao, Y.L., Nguyen, N.T., Presto, A.A., Hennigan, C.J., May, A.A. and Robinson, A.L.: Intermediate volatility organic compound emissions from on-road diesel vehicles: Chemical composition, emission factors, and estimated secondary organic aerosol production, Environ. Sci. Technol., 49, 11516-11526, http://doi.org/10.1021/acs.est.5b02841, 2015.

Zhou, C.F., Jang, M. and Yu, Z.C.: Simulation of SOA formation from the photooxidation of monoalkylbenzenes in the presence of aqueous aerosols containing electrolytes under various NOx levels, Atmos. Chem. Phys., 19, 5719-5735, http://doi.org/10.5194/acp-19-5719-2019, 2019.

Ziemann, P.J. and Atkinson, R.: Kinetics, products, and mechanisms of secondary organic aerosol formation, Chem. Soc. Rev., 41, 6582-6605, http://doi.org/10.1039/c2cs35122f, 2012.